Sulfur $K\beta$ x-ray emission from carbonyl sulfide: Variations with polarization and excitation energy at the S K threshold

K. E. Miyano
Department of Physics, Brooklyn College, Brooklyn, New York 11210

U. Arp
National Institute of Standards and Technology, Gaithersburg, Maryland 20899

S. H. Southworth
Physics Division, Argonne National Laboratory, Argonne, Illinois 60439

Timothy E. Meehan, Tiffany R. Walsh, and Frank P. Larkins
School of Chemistry, The University of Melbourne, Parkville, Australia 3052
(Received 27 October 1997)

Sulfur $K\beta$ x-ray-emission spectra from carbonyl sulfide have been measured with resonant excitation at the sulfur K absorption threshold and compared with results of self-consistent field and singles-doubles configuration-interaction calculations. For excitation to the strong 4π absorption resonance, a splitting of the main emission peak is interpreted in terms of influence of the 4π electron on the final valence-hole states. The polarization selectivity of the emission spectrometer was used to distinguish emission polarized parallel versus perpendicular with respect to the polarization of the excitation radiation. The observed polarization dependence is consistent with the molecular symmetries of the calculated intermediate and final states. [S1050-2947(98)01604-7]

PACS number(s): 33.20.Rm, 31.10.+z, 33.50.Dq

I. INTRODUCTION

The availability of synchrotron radiation as an intense, tunable, polarized x-ray source has stimulated studies of core-valence x-ray emission from gases and solids in the neighborhood of the core excitation threshold [1–3]. The diagram x-ray fluorescence spectrum, which follows photoionization far above threshold, is modified when the excitation energy is tuned below threshold to the region of quasibound excited states. Polarized excitation to states of particular molecular symmetry produces aligned intermediate states and can result in strongly polarized and anisotropic x-ray emission. These effects have been explained using the semiclassical two-step model to relate the molecular symmetries of the states involved to the polarization and propagation directions of the absorbed and emitted x rays [4–6]. Recently, the Kramers-Heisenberg formalism for resonant inelastic x-ray scattering has been applied to develop quantum-mechanical theories of molecular x-ray scattering that show how this two-step model is appropriate in limiting cases [7,8].

The linear carbonyl sulfide (OCS) molecule has 30 electrons, and the ground-state electronic configuration is $1\sigma^2 2\sigma^2 3\sigma^2 4\sigma^2 5\sigma^2 1\pi^4 6\sigma^2 7\sigma^2 8\sigma^2 9\sigma^2 2\pi^4 3\pi^4$. Here 1σ, 2σ, 3σ, 4σ, 5σ, and 1π are associated with S $1s$, O $1s$, C $1s$, S $2s$, S $2p_{1/2}$, and S $2p_{3/2}$ core levels, respectively, while the higher-lying levels are valence states of mixed atomic character. S K x-ray absorption spectra have been measured previously by Perera and LaVilla [9]. Those authors, as well as Mazalov *et al.* [10], have measured diagram S $K\beta$ emission. Furthermore, Mazalov *et al.* reported diagram O $K\alpha$, C $K\alpha$, and S L emission spectra. O $K\alpha$, C $K\alpha$, and S L spectra also have been calculated recently for the diagram and 4π-resonant transitions [11], and the calculated diagram spectra agree well with the measurements. The calculated O $K\alpha$ and C $K\alpha$ resonant spectra were significantly changed from the diagram spectra. These changes were mainly attributed to differences between the electron densities of the final valence-hole states. A similar conclusion was reached for the N_2O molecule [12,13].

In the present paper we report the S $K\beta$ emission spectra of OCS for several excitation energies near the S K absorption threshold. Significant variations in line shape and energy position, as well as substantial polarization dependence, are reported. The diagram and 4π-resonant emission spectra are calculated and compared with the measurements.

II. EXPERIMENT

The measurements were performed at beam line X24A of the National Synchrotron Light Source at Brookhaven National Laboratory [14]. At the S K edge (2472 eV), the theoretical resolution of the beam-line monochromator with its pair of Si(111) crystals is 0.35 eV. The x-ray-emission spectra were measured with a secondary monochromator, which we will call the fluorescence spectrometer, consisting of a bent Si(111) crystal and a position-sensitive proportional counter [15]. The spectrometer has a theoretical resolution of 0.30 eV for 2465-eV S $K\beta$ fluorescence. The peak width of x rays that were elastically scattered from the beam line into the spectrometer indicates that the true combined resolution of the beam-line monochromator and fluorescence spectrometer is about twice the theoretical value. The spectrometer

recorded x rays emitted at 90° with respect to both the incident x-ray beam and the incident polarization direction. The incident x-ray beam has strong linear polarization with its polarization vector $\hat{\varepsilon}_1$ in the horizontal plane. This polarization is enhanced by reflection from the beam line's double-crystal monochromator so that the incident x-ray beam is essentially 100% polarized. The fluorescence spectrometer was mounted on a rotatable flange, thus allowing the dispersion plane to be rotated for measurements of the polarization dependence of the emission spectra [4]. We measured emitted x rays with their polarization vector $\hat{\varepsilon}_2$ oriented parallel to $\hat{\varepsilon}_1$, and we separately measured emission with $\hat{\varepsilon}_2$ perpendicular to $\hat{\varepsilon}_1$. The polarization selectivity of the spectrometer for S $K\beta$ fluorescence was 15% of the π-polarized x rays relative to 100% for the σ-polarized component [15].

The incident x rays were focused through a gas cell containing 60 Torr of OCS. Electrical currents from carbon foils before and after the cell are proportional to the incident and transmitted x-ray flux. The transmitted flux was normalized to the incident flux and plotted versus incident photon energy to establish the OCS absorption spectrum. The gas cell has polypropylene windows in line with the incident beam and another window at 90° for passage of emitted x rays to the fluorescence spectrometer. The energy scale of the absorption and emission spectra was established as follows. The main sharp peak of the absorption spectrum, the 4π resonance, was calibrated as 2472.0 eV, after Perera and LaVilla [9]. Having fixed this energy, the well-established dispersion of the beam-line monochromator with Si(111) crystals determined the energy scale of the absorption spectrum. With photon energies from the beam-line monochromator thus established and the fluorescence spectrometer positioned to record S $K\beta$ emission, the gas cell was filled with 1 atm of Ar, and the energy scale of the emission spectrometer was determined from the position of the elastically scattered x-ray peak as the incident energy was adjusted over the spectrometer range. Variations in spectrometer sensitivity were also determined with these Ar elastic-scattering measurements. The spectrometer sensitivity variations were observed to be approximately the same with the detector in its orientations to measure parallel and perpendicular polarizations. Since the elastically scattered peak was weak for the perpendicular orientation, all spectra were normalized to the detector-sensitivity profile determined for the parallel spectrometer orientation.

III. CALCULATION

We have calculated emission spectra, without polarization discrimination, for an excitation energy far above threshold and for excitation at the 4π resonance. It is convenient to perform calculations for the linear OCS molecule in the Abelian C_{2v} subgroup of $C_{\infty v}$. *Ab initio* calculations were undertaken at the Hartree-Fock level to obtain all of the fully optimized initial- and final-state wave functions, using the program CLUSTER [11,16]. All wave functions were calculated at the equilibrium ground-state experimental geometry [17] with a C-O distance of 2.1924 a.u. and a C-S distance of 2.9481 a.u. A Gaussian basis set [18] of Huzinaga $(9s5p)$ functions for carbon and oxygen was used with split d functions (C, $\zeta = 1.845, 0.547$; O, $\zeta = 2.091, 0.619$) and was contracted to $[5s3p2d]$ [19]. For sulfur, a set of $(12s7p)$ Gaussian functions was used, also augmented with split d functions [20] and contracted to $[9s5p2d]$ [19,21]. The open-shell states were calculated using coupling coefficients derived from the energy expressions [22], except for the states arising from two open shells in doubly degenerate orbitals [23]. The absolute transition probabilities were calculated at the relaxed Hartree-Fock (RHF) level, using a multicenter approach as in previous work [11,12].

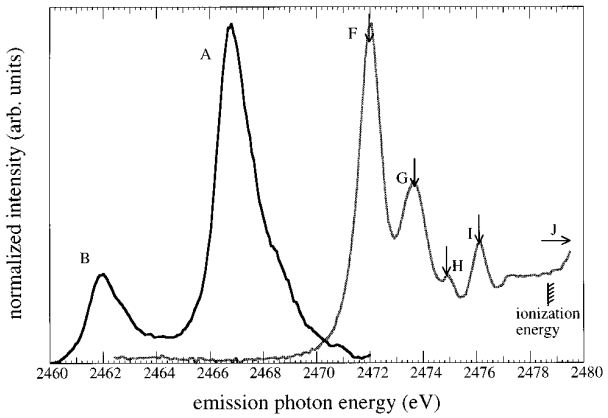

FIG. 1. The S K absorption spectrum is plotted along with a sulfur S K emission spectrum. The emission spectrum was taken with an excitation energy of 2502 eV and with the spectrometer oriented to select $\hat{\varepsilon}_2$ parallel to $\hat{\varepsilon}_1$. Arrows indicate the excitation energies for the near-threshold emission spectra plotted in Fig. 2.

Since the self-consistent field (ΔSCF) ionization energies produce an incorrect ordering for the orbital energies, singles-doubles configuration-interaction (ΔSDCI) calculations were performed using the GAMESS program [24] to determine the energies of the diagram and 4π-resonant emission lines more accurately. For the diagram final states the SDCI calculations were performed in C_{4v} symmetry, and the 7σ-3π valence orbitals and the 4π and 10σ virtual orbitals were active in the CI space. The reference function for the OCS $[2\pi]$ and $[3\pi]$ valence holes was the RHF OCS$[3p]$ wave function. The reference function for the OCS $[7\sigma]$, $[8\sigma]$, and $[9\sigma]$ valence holes was the RHF OCS$[9s]$ wave function. For the diagram initial state, the 1σ orbital replaced the 7σ valence orbital in the CI active space, and the RHF OCS$[1\sigma]$ wave function was the reference function. For the 4π-resonant states, the SDCI was performed in $C1$ symmetry and a multiplicity of one, with the same active spaces of the diagram CI calculations. C1 symmetry was used to obtain all of the final states of each symmetry. For the resonant final state, the RHF OCS$[3\pi]$ wave function was used as reference function to include relaxation effects due to the valence hole. For the resonant initial state, the RHF OCS$[1\sigma]$ wave function was used as the reference function to include the relaxation due to the core hole.

IV. RESULTS AND DISCUSSION

Figure 1 shows the present measurements of the S K absorption and diagram S $K\beta$ emission spectra from OCS. The indicated S K ionization energy 2478.7 eV was established by Perera and LaVilla [9], who combined photoemission binding energies with x-ray-emission energies. The diagram

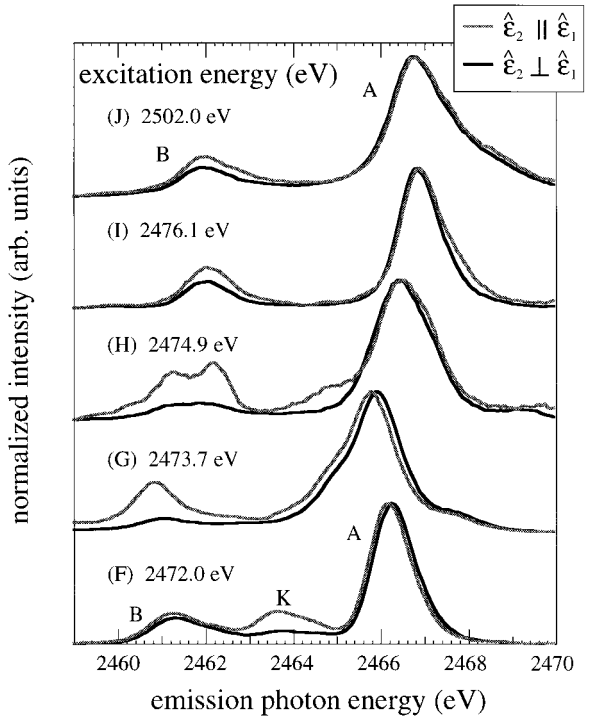

FIG. 2. S *K*-valence emission is shown for five excitation energies near and above the S *K* absorption threshold. Separate spectra are shown for polarization vector $\hat{\varepsilon}_2$ oriented parallel to the excitation polarization vector $\hat{\varepsilon}_1$ (labeled $\hat{\varepsilon}_2 \| \hat{\varepsilon}_1$) and for $\hat{\varepsilon}_2$ perpendicular to $\hat{\varepsilon}_1$ (labeled $\hat{\varepsilon}_2 \perp \hat{\varepsilon}_1$).

emission spectrum in Fig. 1 is similar to that reported in Ref. [9], and the same labeling of peaks is used. Figure 1 indicates the excitation energies at which resonant emission spectra were recorded, at peaks *F*, *G*, *H*, and *I* of the absorption spectrum. The excited states associated with peaks *F*, *G*, and *H* are 4π, 10σ, and 11σ, respectively, while peak *I* is suggested to be a transition to the $4p$ Rydberg state of the S $1s$ hole [9]. Figure 2 shows the emission spectra taken at the excitation peaks *F*, *G*, *H*, and *I* at 2472.0, 2473.7, 2474.9, and 2476.1 eV, respectively, as well as an excitation energy of 2502 eV, i.e., far above threshold. For simplicity, we will refer to the emission spectra associated with peak *F* in the absorption spectrum as emission spectra *F*, and so on. The spectra excited near threshold are substantially different in both line shape and energy position, and a polarization dependence is clearly observed.

The ΔSCF line energies and transition probabilities for the length and velocity forms of the dipole operator are presented in Table I. The more accurate ΔSDCI energies are presented in Tables II and III for the diagram and 4π-resonant transitions, respectively, and the major CI coefficients are also listed for each state. For both the diagram and 4π-resonant emission spectra, calculated lines, based on ΔSDCI energies and ΔSCF intensities, are overlaid in Fig. 3 on measured spectra.

A. Diagram emission spectra

As mentioned above, the emission spectra *J*, excited far above threshold at 2502 eV, are similar to that reported by Perera and LaVilla [9] and represent the characteristic dia-

TABLE I. Comparison of the ΔSCF line energies and absolute intensities for the diagram and 4π-resonant S $K\beta$ emission spectra of the OCS molecule.

Initial state	Final state	ΔE (eV)	A_1 (10^{-6} a.u.)[a]	A_v (10^{-6} a.u.)[b]
$[1\sigma]$	$[6\sigma]$	2437.2	0.12	0.19
$[1\sigma](4\pi)$	$[6\sigma](4\pi)$	2436.7	0.22	0.39
$[1\sigma]$	$[7\sigma]$	2446.3	1.93	2.63
$[1\sigma](4\pi)$	$7\sigma](4\pi)$	2445.3	1.05	2.75
$[1\sigma]$	$[8\sigma]$	2457.8	1.67	1.41
$[1\sigma](4\pi)$	$[8\sigma](4\pi)$	2456.9	3.11	2.63
$[1\sigma]$	$[2\pi]$	2458.2	13.32	12.10
$[1\sigma](4\pi)$	$[2\pi](4\pi)\Sigma^+$	2452.1	7.21	6.49
$[1\sigma](4\pi)$	$[2\pi](4\pi)\Sigma^-$	2458.0	16.49	14.82
$[1\sigma](4\pi)$	$[2\pi](4\pi)\Delta$	2457.6	17.18	14.45
$[1\sigma]$	$[9\sigma]$	2458.3	20.13	16.06
$[1\sigma](4\pi)$	$[9\sigma](4\pi)$	2456.8	26.30	19.08
$[1\sigma]$	$[3\pi]$	2463.8	78.41	71.63
$[1\sigma](4\pi)$	$[3\pi](4\pi)\Sigma^+$	2461.4	79.24	71.85
$[1\sigma](4\pi)$	$[3\pi](4\pi)\Sigma^-$	2462.9	75.48	68.30
$[1\sigma](4\pi)$	$[3\pi](4\pi)\Delta$	2463.8	76.61	69.33
$[-]$	$[1s]$	2474.3		
$[1\sigma](4\pi)$	$[-]$	2468.3	14.78	13.56
totals				
$[1\sigma]$			115.58	104.02
$[1\sigma](4\pi)$	spectator		302.89	271.09
$[1\sigma](4\pi)$	total		317.67	284.65

[a] A_1 is the length form of the dipole operator.

[b] A_v is the velocity form of the dipole operator.

TABLE II. Diagram ΔSDCI energies with the major coefficients of the contributing determinants.

SDCI states	Major determinants	ΔE (eV)
$[3\pi]$	$+0.961[3\pi_y]$	2466.0
$[2\pi]$	$+0.838[2\pi_y]-0.309[2\pi_y,3\pi_y](4\pi_y)+0.263[2\pi_y,3\pi_x](4\pi_x)$	2461.1
$[9\sigma]$	$+0.942[9\sigma]$	2461.0
$[8\sigma]$	$+0.822[8\sigma]+0.313[8\sigma,3\pi_x](4\pi_x)+0.313[8\sigma,3\pi_y](4\pi_y)$	2457.8
$[1\sigma]$	$+0.973[1\sigma]$	

gram fluorescence. As demonstrated by the calculated lines in Fig. 3, the peak labeled *A* corresponds to a $[3\pi]$ final state, while peak *B* corresponds to an admixture of $[9\sigma]$ and $[2\pi]$ final states. The emission spectra *I*, excited at 2476.1 eV, are similar to spectra *J* in both energy position and line shape, except that the high-energy shoulders, due to multivacancy satellites, have been suppressed [25]. The fluorescence spectra excited far above threshold are anticipated to have little polarization dependence [4,5]. Excitation to continuum states constituting a mixture of symmetries yields excited molecules with little alignment. The slight increase in the *B*-to-*A* intensity ratio when comparing parallel to perpendicular is thus attributed to an instrumental factor: the sensitivity variation across the detector, which was assumed to be exactly the same for the two detector orientations, is believed to cause this difference.

The ΔSCF transition energies in Table I are approximately 4 eV lower than corresponding experimental energies. This is due to the discrepancy in the ionization potential of the 1σ orbital, which at the ΔSCF level is 4 eV too low [9,11,26]. When electron correlation is included (Tables II and III), the transition energies show better agreement with the experimental values. In Fig. 3 the ΔSDCI-calculated lines have been shifted up by 0.9 eV for best comparison to the measured spectra. Further refinement of the CI calculation, i.e., higher-order CI or a larger basis set, may provide better absolute energy agreement with experiment, but relativistic effects may also contribute to the discrepancies. The calculated relative intensities agree well with experiment. The $[3\pi]$ transition is predicted to be the most intense, while the combined $[9\sigma]+[2\pi]$ transition has significant intensity. The weak peak *C* in the emission data of Perera of LaVilla [9] (not measured in the present experiment) is attributed to a $[8\sigma]$ transition, and the calculations (Table I) predict it to be of low intensity.

B. 4π resonant emission spectra

As shown in Fig. 3, the measured and calculated 4π-resonant emission spectra differ substantially from the diagram spectra. The resonant spectra are shifted down in energy, and peak *A* from the diagram spectrum has split into peaks *A* and *K* in the measured resonant spectrum. The calculation attributes this splitting to the separation of the $[3\pi](4\pi)$ states into Σ^+, Σ^-, and Δ states: peak *A* consists of the combined $[3\pi](4\pi)$ Σ^- and Δ transitions, while peak *K* is the $[3\pi](4\pi)\Sigma^+$ transition. From the CI calculation, we note that the $[3\pi](4\pi)\Sigma^+$ state mixes substantially with the $[9\sigma](10\sigma)$ state; thus the $[3\pi](4\pi)\Sigma^+$ energy is higher with respect to the $[3\pi](4\pi)$ Σ^- and Δ states, yielding a lower transition energy. This CI state may not be adequately described since the calculated line is at lower energy than measured peak *K*. Peak *B* is the combined $[9\sigma](4\pi)$ $+[2\pi](4\pi)$ Σ^- and Δ transitions. In the calculation there is also a low-intensity transition centered at 2456.3 eV (Table III). This arises from the $[2\pi](4\pi)\Sigma^+$ transition, which is lower in energy than the $[2\pi](4\pi)$ Σ^- and Δ transitions, again due to mixing with the $[9\sigma](10\sigma)$ state.

The calculations indicate that the $[9\sigma](4\pi)+[2\pi](4\pi)$ Σ^- and Δ transitions have higher absolute intensities than the analogous diagram transitions, while the $[3\pi](4\pi)$ Σ^- and Δ transitions have a lower absolute intensity than the analogous diagram transition. In earlier work [11], similar changes were calculated for the oxygen *K* and carbon *K* transitions, and the changes were attributed to rearrangements in the final-state electron density. The $[2\pi](4\pi)\Sigma^-$ final state has less electron density around the carbon atom than the diagram $[2\pi]$ final state, and the absolute transition rate for the resonant case decreases significantly. The sulfur atom, however, has a substantial increase in density for the $[2\pi](4\pi)\Sigma^-$ final state, and the absolute transition rate is

TABLE III. 4π-resonant ΔSDCI energies with the major coefficients of the contributing determinants.

SDCI states	Major determinants	ΔE (eV)
g.s. Σ^+	$+0.975[-]$	2472.5
$[3\pi](4\pi)\Delta$	$+0.686[3\pi_x](4\pi_y)-0.686[3\pi_y](4\pi_x)$	2465.5
$[3\pi](4\pi)\Sigma^-$	$+0.688[3\pi_x](4\pi_y)+0.688[3\pi_y](4\pi_x)$	2465.5
$[3\pi](4\pi)\Sigma^+$	$-0.610[3\pi_y](4\pi_y)+0.610[3\pi_x](4\pi_x)-0.399[9\sigma](10\sigma)$	2461.6
$[2\pi](4\pi)\Sigma^-$	$+0.635[2\pi_x](4\pi_y)+0.635[2\pi_y](4\pi_x)$	2460.7
$[2\pi](4\pi)\Delta$	$-0.625[2\pi_x](4\pi_y)+0.625[2\pi_y](4\pi_x)$	2460.7
$[9\sigma](4\pi)$	$+0.848[9\sigma](4\pi_x)-0.315[9\sigma](4\pi_y)-0.224[3\pi_x](10\sigma)$	2459.6
$[8\sigma](4\pi)$	$+0.767[8\sigma](4\pi_x)+0.377[8\sigma](4\pi_y)$	2456.9
$[2\pi](4\pi)\Sigma^+$	$-0.481[2\pi_y](4\pi_y)+0.481[2\pi_x](4\pi_x)+0.361[9\sigma](10\sigma)$	2456.3
$[1\sigma](4\pi)$	$+0.761[1\sigma,3\pi_y](4\pi_y)-0.631[1\sigma,3\pi_y](4\pi_x)$	

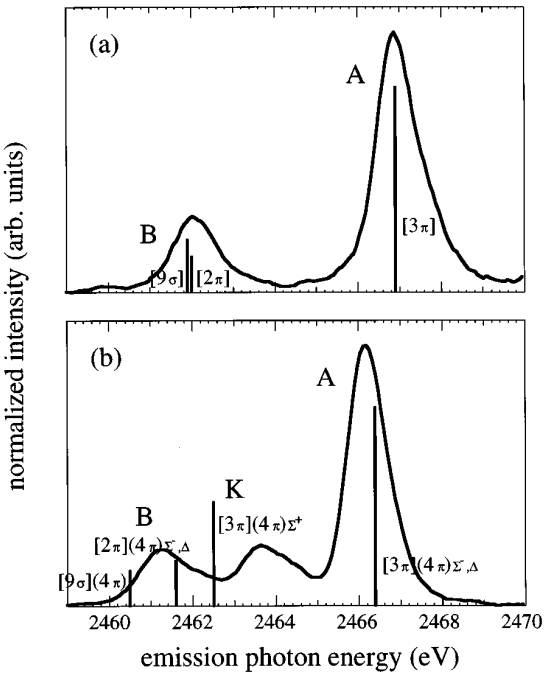

FIG. 3. Calculated emission lines are overlaid on measured spectra. In (a) the emission spectrum, excited at 2476.1 eV, represents a diagram spectrum without contamination by multihole satellites. In (b) the emission spectrum, excited at 2472.0 eV, represents a 4π-resonant spectrum. The measurements in (a) and (b) correspond to $\hat{\varepsilon}_2$ parallel to $\hat{\varepsilon}_1$. The calculated lines have been shifted up by 0.9 eV from the values in Tables II and III.

calculated to be higher than the diagram absolute rate. As shown in Table I, the $[3\pi](4\pi)\Sigma^+$ intensity is calculated to be significant. However, at this SCF level the calculated relative intensity is high compared to experiment: peak *K* in Fig. 2 has a lower integrated intensity than peak *B*, whereas the combined calculated absolute intensity of the $[9\sigma](4\pi)+[2\pi](4\pi)\ \Sigma^-$ and Δ transitions is 59.97×10^{-6} a.u. compared to 79.24×10^{-6} a.u. for the $[3\pi](4\pi)\Sigma^+$ transition. Correlated calculations of the absolute transition probabilities should improve the relative intensities, but the peak assignments from the ΔSDCI calculations are in reasonable agreement with experiment.

C. Other resonant emission spectra

The 10σ-resonant emission spectra, which follow excitation to absorption peak *G* at 2473.7 eV, are shifted even further down in energy and do not exhibit the intermediate-energy peak *K*. The low-energy emission peak here has a very strong polarization dependence. The 11σ-resonant emission spectra, which follow excitation to absorption peak *H* at 2474.9 eV, exhibit a similar polarization dependence, although they are broader and are less shifted to lower energy. The broadness of these spectra are possibly due to substantial excitation of states other than 11σ, yielding a partial emission contribution similar to the spectra *I*.

D. Polarization dependence

The polarization dependence of the 4π-resonant emission spectra [Fig. 2 (*F*)] can be explained qualitatively using the classical two-step model to relate the intermediate and final-state molecular symmetries to the directions of the incident and emitted x-ray polarization vectors $\hat{\varepsilon}_1$ and $\hat{\varepsilon}_2$ [4,5]. The entries of Table III for final states $[3\pi](4\pi)\ \Sigma^-$ and Δ, which correspond to peak *A* in Fig. 2 (*F*), involve determinants such as $[3\pi_x](4\pi_y)$ for which the emission dipole moment is *perpendicular* to the absorption dipole. Similarly, the determinants in Table III for final states $[9\sigma](4\pi)+[2\pi](4\pi)\ \Sigma^-$ and Δ indicate that for peak *B* in Fig. 2 (*F*), the emission dipole is perpendicular to the absorption dipole. Thus we expect the transitions of peaks *A* and *B* to be preferentially emitted perpendicular to the polarization of the incident x-ray beam. In contrast, the entry in Table III for the final state $[3\pi](4\pi)\Sigma^+$, which corresponds to peak *K* in Fig. 2 (*F*), involves determinants such as $[3\pi_y](4\pi_y)$, for which the emission dipole is *parallel* to the absorption dipole.

Quantitatively, we take the classical values for the emission anisotropy *R* [5] and arrive at the following predictions for the ratio of the parallel emission intensity to the perpendicular emission intensity: $I_\parallel/I_\perp=0.5$ for peaks *A* and *B*, while $I_\parallel/I_\perp=3$ for peak *K*, and these are modified by our limited (85%) polarization selectivity to 0.6 and 2.2, respectively. In Fig. 2 the parallel and perpendicular spectra are normalized to the same intensity for peak *A*. With such normalization the above numbers predict that peak *K* will be 3.7 times stronger for the parallel polarization direction, while peak *B* is not expected to vary. In Fig. 2 the intensities of peak *B* do roughly match. The measured enhancement of peak *K* is difficult to quantify because of the overlapping tails of the stronger peaks *A* and *B*. Results of peak fitting indicate that the measured enhancement for peak *K* is 3 times, in approximate agreement with the prediction. The polarization dependencies observed in the emission spectra of Fig. 2 (*G*) and (*H*) are similarly expected to reflect the symmetries of the intermediate and final states.

V. CONCLUSIONS

S $K\beta$ x-ray-emission spectra from OCS have been recorded at the S *K* threshold. Excitation to 4π, 10σ, and 11σ states at the threshold yield substantial changes in energy position and line shape. Moreover, when the threshold-excited spectra are recorded separately for parallel and perpendicular polarization selectivity, marked differences are observed. The line shape and polarization variations of the 4π-resonant emission spectrum have been understood, based on ΔSCF intensity and ΔSDCI energy calculations. In particular, the presence of the 4π electron in the final state yields $[3\pi](4\pi)\ \Delta$, Σ^-, and Σ^+ valence-hole states of marked energy separation, and this energy separation in turn allows observation of polarization differences for transitions to these resonant final states. Future theoretical studies of this system can include additional correlation and relativistic effects and extending the calculations to the other resonant transitions recorded near threshold.

ACKNOWLEDGMENTS

The authors thank B. A. Karlin for technical assistance U.A. is grateful for financial support by the Alexander von Humboldt Foundation. This work was supported by the U.S. Department of Energy, Office of Basic Energy Sciences under Contract No. W-31-109-ENG-38.

[1] J. Nordgren, in *New Directions in Research with Third-Generation Soft X-Ray Synchrotron Sources*, edited by A. S. Schlachter and F. J. Wuilleumeier (Kluwer, Dordrecht, 1994), p. 189.

[2] D. L. Ederer, K. E. Miyano, W. L. O'Brien, T. A. Callcott, Q.-Y. Dong, T. A. Callcott, D. R. Mueller, J.-E. Rubensson, R. C. C. Perera, and R. Shuker, in *New Directions in Research with Third-Generation Soft X-Ray Synchrotron Sources* (Ref. [1]), p. 281.

[3] *Raman Emission by X-Ray Scattering*, edited by D. L. Ederer and J. H. McGuire (World Scientific, Singapore, 1996).

[4] D. W. Lindle, P. L. Cowan, T. Jach, R. E. La Villa, R. D. Deslattes, B. Karlin, J. A. Sheehy, T. J. Gil, and P. W. Langhoff, Phys. Rev. Lett. **60**, 1010 (1988); D. W. Lindle, P. L. Cowan, T. Jach, R. E. La Villa, R. D. Deslattes, and R. C. C. Perera, Phys. Rev. A **43**, 2353 (1991).

[5] S. H. Southworth, D. W. Lindle, R. Mayer, and P. L. Cowan, Phys. Rev. Lett. **67**, 1098 (1991); S. H. Southworth, D. W. Lindle, R. Mayer, and P. L. Cowan, Nucl. Instrum. Methods Phys. Res. B **56/57**, 304 (1991).

[6] R. Mayer, D. W. Lindle, S. H. Southworth, and P. L. Cowan, Phys. Rev. A **43**, 235 (1991).

[7] Y. Luo, H. Ågren, and F. Gel'mukhanov, Phys. Rev. A **53**, 1340 (1996).

[8] J. D. Mills and P. W. Langhoff, in *Raman Emission by X-Ray Scattering* (Ref. [3]), p. 169.

[9] R. C. C. Perera and R. E. La Villa, J. Chem. Phys. **81**, 3375 (1984).

[10] L. N. Mazalov, A. P. Sadovskii, E. S. Gluskin, G. N. Dolenko, and A. A. Krasnoperova, Zh. Strukt. Kh. **15**, 800 (1974) [J. Struct. Chem. **15**, 705 (1974)].

[11] T. R. Walsh, T. E. Meehan, and F. P. Larkins, J. Phys. B **29**, 207 (1996).

[12] T. E. Meehan, K. Hermann, and F. P. Larkins, J. Phys. B **28**, 357 (1995).

[13] T. E. Meehan and F. P. Larkins, J. Phys. B **28**, 1673 (1995).

[14] P. L. Cowan, S. Brennan, R. D. Deslattes, A. Henins, T. Jach, and E. G. Kessler, Nucl. Instrum. Methods Phys. Res. A **246**, 154 (1986).

[15] S. Brennan, P. L. Cowan, R. D. Deslattes, A. Henins, D. W. Lindle, and B. A. Karlin, Rev. Sci. Instrum. **60**, 2243 (1989).

[16] K. Hermann, SCF CLUSTER program, Fritz-Haber Institute, Berlin, 1992.

[17] *Interatomic Distances*, edited by L. E. Sutton (London Chemical Society, London, 1965), Suppl. 1956–1959.

[18] T. H. Dunning, J. Chem. Phys. **53**, 2823 (1970).

[19] T. H. Dunning, J. Chem. Phys. **55**, 3958 (1971).

[20] *Gaussian Basis Sets for Molecular Calculations*, edited by S. Huzinaga (Elsevier, Amsterdam, 1984).

[21] A. Veillard, Theor. Chim. Acta **12**, 405 (1968).

[22] R. Carbo and J. M. Riera, in *A General SCF Theory*, edited by G. Berthier *et al.* Lecture Notes in Chemistry Vol. 5 (Springer-Verlag, New York, 1978).

[23] J. B. Rose and V. McKoy, J. Chem. Phys. **55**, 5435 (1971).

[24] M. W. Schmidt, K. K. Baldridge, J. A. Boatz, S. T. Elbert, M. S. Gordon, J. H. Jensen, S. Koseki, N. Matsunaga, K. A. Nguyen, S. Su, T. L. Windus, M. Dupuis, and J. A. Montgomery, J. Comput. Chem. **14**, 1347 (1993).

[25] R. D. Deslattes, R. E. LaVilla, P. L. Cowan, and A. Henins, Phys. Rev. A **27**, 923 (1983).

[26] C. J. Allan, U. Gelius, D. A. Allison, G. Johannsson, H. Siegbahn, and K. Siegbahn, J. Electron Spectrosc. Relat. Phenom. **1**, 131 (1972).